electronics

MDPI

Article

Joint Optimization of Renewable Energy Utilization and Multi-Energy Sharing for Interconnected Microgrids with Carbon Trading

Jieqi Rong [1], Weirong Liu [1,*], Nvzhi Tang [2], Fu Jiang [2], Rui Zhang [3] and Heng Li [2]

[1] School of Computer Science and Engineering, Central South University, Changsha 410083, China; rongjieqi@csu.edu.cn
[2] School of Electronic Information, Central South University, Changsha 410083, China; tnz-starlight@csu.edu.cn (N.T.); jiangfu@csu.edu.cn (F.J.); liheng@csu.edu.cn (H.L.)
[3] School of Electronic Information and Electrical Engineering, Changsha University, Changsha 410022, China; ruizhang@ccsu.edu.cn
* Correspondence: frat@csu.edu.cn

Abstract: Connecting microgrids can promote the sharing of multi-energy sources, reduce carbon emissions, and enhance the consumption of renewable energy. However, the uncertainty of renewable energy and the coupling of multiple energy sources makes energy management difficult in connected microgrids. To address the challenges, a dual-layer energy management framework for interconnected microgrids is proposed in this paper. In the bottom layer, a load scheduling problem within one microgrid is formulated to maximize the utilization of renewable energy, which is solved by an improved gray wolf algorithm with fast convergence and effective optimum seeking. In the upper layer, a distributed energy dispatch strategy is proposed to coordinate the energy sources for multiple microgrids to achieve multi-energy sharing with carbon trading. Combining the load scheduling and energy dispatching, the overall energy utilization is improved, and the operation cost and carbon emission are reduced. The simulation results on real-world datasets validate the effectiveness of the proposed method.

Keywords: interconnected microgrids; load scheduling; energy dispatching; multi-energy sharing; renewable energy utilization; carbon trading

Citation: Rong, J.; Liu, W.; Tang, N.; Jiang, F.; Zhang, R.; Li, H. Joint Optimization of Renewable Energy Utilization and Multi-Energy Sharing for Interconnected Microgrids with Carbon Trading. *Electronics* **2024**, *13*, 4995. https://doi.org/10.3390/electronics13244995

Academic Editor: José Matas

Received: 9 November 2024
Revised: 13 December 2024
Accepted: 18 December 2024
Published: 19 December 2024

1. Introduction

In recent years, the issues of energy shortages and environmental pollution have attracted much public attention. To reduce the use of fossil fuels and carbon emissions, large-scale clean renewable energy sources and multi-energy are integrated into the microgrid system to achieve stable and reliable operation [1,2]. Microgrids (MGs) typically operate in a grid-connected mode. However, in remote areas where connecting to the main grid is inconvenient, microgrids play a crucial role in energy supply [3]. However, individual microgrids are less resistant to interference, being liable to system collapse in fault occurrence [4]. Interconnected microgrids break through the limitations of the individual microgrid and strengthen the robustness of microgrids [5]. The connection of microgrids has been validated as an effective approach to achieve stable system operation, enhance resilience, reduce carbon emission, and improve the utilization of large-scale distributed renewable energy sources [6].

Within one microgrid, renewable energy utilization can be promoted by means of load scheduling. There are many studies that regulate flexible loads to reduce the operation cost as much as possible under the regulatable range. In [7], a decentralized gradient projection method is proposed for solving the economic load dispatch problem of thermal power units. In [8], a microgrid air conditioning load scheduling model is developed and a stochastic

robust optimization model is solved using a column constraint generation algorithm. In [9], a multi-objective residential load scheduling strategy is proposed and the load scheduling problem is transformed into a mixed-integer programming problem to be solved. However, although these traditional methods are effective in solving fundamentally convex objective functions, they are less effective in solving high-dimensional variables or nonconvex and nonsmooth objectives in such optimization problems.

Thus, meta-heuristic intelligent algorithms are proposed to solve the load scheduling issue of microgrids. For instance, the genetic algorithm is utilized for residential load shifting, which takes into account distributed generation and dynamic pricing. This approach aims to minimize energy costs, and consequently, reduce electricity bills [10]. In [11], the dragonfly algorithm is proposed to solve the economic load dispatch problem in power systems. In [12], a nondominated sorting genetic algorithm is used as a multi-objective optimization algorithm for residential load scheduling methods for smart grids. In meta-heuristic intelligent algorithms, the gray wolf optimization algorithm has the potential and effectiveness to achieve global optimization in the power system, and it has a better transfer mechanism and information-sharing ability, which provides a more diversified solution space search for solving the complex economic load scheduling problems [13,14]. However, the convergence speed and search capability of the original gray wolf algorithm still need to be improved to meet the requirements of real-time scheduling.

Furthermore, when microgrids are connected, it is preferable to share the various energy resources among microgrids, improving energy efficiency. In terms of energy sharing, a two-layer optimal allocation method is proposed for microgrids with the aid of shared electric hydrogen storage stations in [15]. In [16], a green power value-driven energy sharing approach for interconnected microgrids is proposed. In [17], the interactions between interconnected microgrids are investigated and the incentive mechanisms are developed by using Nash bargaining theory to encourage energy trading and sharing. Nevertheless, only the electrical energy is shared among microgrids in the above research. Currently, more and more microgrids are integrating multiple energies; the sharing and transferring of multiple energies should be of most concern.

Many economic dispatch algorithms scheduling energy sources have emerged in the field of energy optimization with centralized modes [18,19]. The multi-energy coupling in multi-microgrid systems, coupled with the diversity of energy devices, presents a significant challenge to energy dispatch. This challenge complicates the application of previous centralized algorithms. Thus, some distributed dispatch methods have been developed recently, which can provide more robust, economical, and efficient scheduling for distributed power systems [20]. In [21], a fully distributed framework using the analytic target cascading approach was proposed and applied to energy dispatch for multi-microgrid systems. A multiplier-based proto-dyadic method to implement a distributed optimization approach is used to model a transportation system for smart islands to save energy and minimize operating costs [22]. However, the above-distributed methods have the same problem in terms of optimality. In the distributed optimal algorithms, the alternating direction method of multipliers is shown to exhibit superior performance on the optimal capability and convergence speed [23,24].

The joint optimization of load scheduling and energy dispatching enables the efficient and rational utilization of energy as well as the stable and economic operation of the microgrid system. There is some literature in existing research that studies joint load optimization and energy dispatch in microgrids. A generic energy optimization model is proposed for the grid-connected integrated energy systems, considering price-based demand response and incentive-based demand response, respectively [25]. In [26], a control algorithm is introduced to manage the combined challenges of demand response and thermal comfort within microgrids, utilizing renewable energy and energy storage units. Additionally, ref. [27] presents an optimal control framework aimed at coordinating building HVAC systems, renewable energy sources, and peak load reduction, all while maintaining user comfort. In [28], an integrated optimal control strategy is proposed that

synergistically combines demand-side management with a grid-tied microgrid approach to effectively handle the supply and demand aspects of the grid.

However, for interconnected multi-microgrid systems, the direct joint optimization of load scheduling and energy dispatching can lead to a complex scenario characterized by a high number of dimensions and a multitude of interdependent constraints, often culminating in complex optimization problems. Thus, it is worth investigating the combination framework to jointly optimize the load scheduling and energy dispatching under interconnected multi-microgrids.

Carbon emission plays a critical role in energy management, which is emphasized by [29]. Interconnected microgrids have been shown to be effective in reducing the carbon emissions of the system through the rationalization of energy utilization. In [20], an optimization model was developed that integrates the minimization of both energy costs and carbon emissions, and a two-tier scheduling model for multi-energy systems was proposed. In [30], a charging strategy for electric vehicles was proposed that aligns with carbon emission constraints. In [31], a stochastic planning model for a multi-energy multi-microgrid network was developed with a focus on low-carbon considerations.

However, these methods are hard to dynamically adapt to the fluctuating energy demands and supply scenarios characteristics of an interconnected microgrid. And addressing the complexities of synthesizing the conversion of multiple energy forms and integrating carbon trading to mitigate the constraints imposed by carbon emission limits is a considerable challenge.

To address the above issues, a dual-layer energy management framework for interconnected microgrids is proposed to integrate the load scheduling of the demand side and dispatching of the multi-energy resources. The energy management strategy includes two layers: the electric load scheduling of the demand side based on an improved gray wolf algorithm, and the energy dispatching based on a distributed algorithm, considering multi-energy sharing and carbon trading. In the bottom layer, load scheduling is developed to redistribute the electric load and to make use of renewable energy fully. In the upper layer, the dispatching problem with multi-energy sharing and carbon trading between interconnected microgrids is solved by using the distributed alternating direction method of multipliers. The proposed strategy can improve the utilization of multiple forms of energy and achieve a low-carbon economic operation of interconnected microgrid networks. The main contributions of this paper are as follows:

- A dual-layer load scheduling and energy dispatching joint optimization energy management framework is proposed to optimize the operation cost and reduce carbon emission for multi-energy interconnected microgrids.
- An improved gray wolf optimization algorithm using backward learning, Cauchy variance, and the nonlinear convergence factor is developed to solve the load scheduling problem and maximize renewable energy utilization.
- Multi-energy sharing and carbon trading are considered in energy dispatching and the alternating direction method of multipliers is utilized to solve the dispatch problem in distributed mode.

The remainder of this paper is organized as follows: Section 2 presents the system framework and mathematical model, including the structure of the interconnected microgrids system, the unit models, and the optimization problem. In Section 3, the electric load scheduling and energy dispatching strategy are presented in detail. In Section 4, the dual-layer energy optimization management simulation results of interconnected microgrids are conducted and analysed. Finally, the work is concluded and future perspectives of research are presented in Section 5.

2. Energy Management Framework and System Modeling

In this section, the interconnected microgrids framework and various energy devices are modeled first. Then, the renewable energy resource maximum utilization and load scheduling model are described in detail. The dual-layer energy management framework

is proposed by combining the bottom-layer electric load scheduling for individual microgrids and the upper-layer energy dispatching for interconnected microgrids, including the dispatch of electrical and thermal energy of locally controllable units, energy sharing, and carbon quota trading. At the same time, the constraints of each energy equipment and the supply–demand balance of the interconnected microgrids system are satisfied.

2.1. Model of Interconnected Multi-Microgrids

The interconnected multi-microgrids system consists of several MGs (MG1, MG2, ..., MG_N). These microgrids are defined as $\mathcal{N}$, $\mathcal{N} = \{1, 2, \ldots, N\}$. Each MG in the interconnected multi-microgrids network is indexed by $i \in \mathcal{N}$. As shown in Figure 1, in each microgrid, there are renewable energy sources (RES), combined heat and power units (CHP), gas boilers (GB), energy storage systems (ES), conventional generators (CG), and loads. To achieve the maximum consumption of renewable energy, surplus renewable electricity can be stored or transmitted to other MGs to meet the system's load demand.

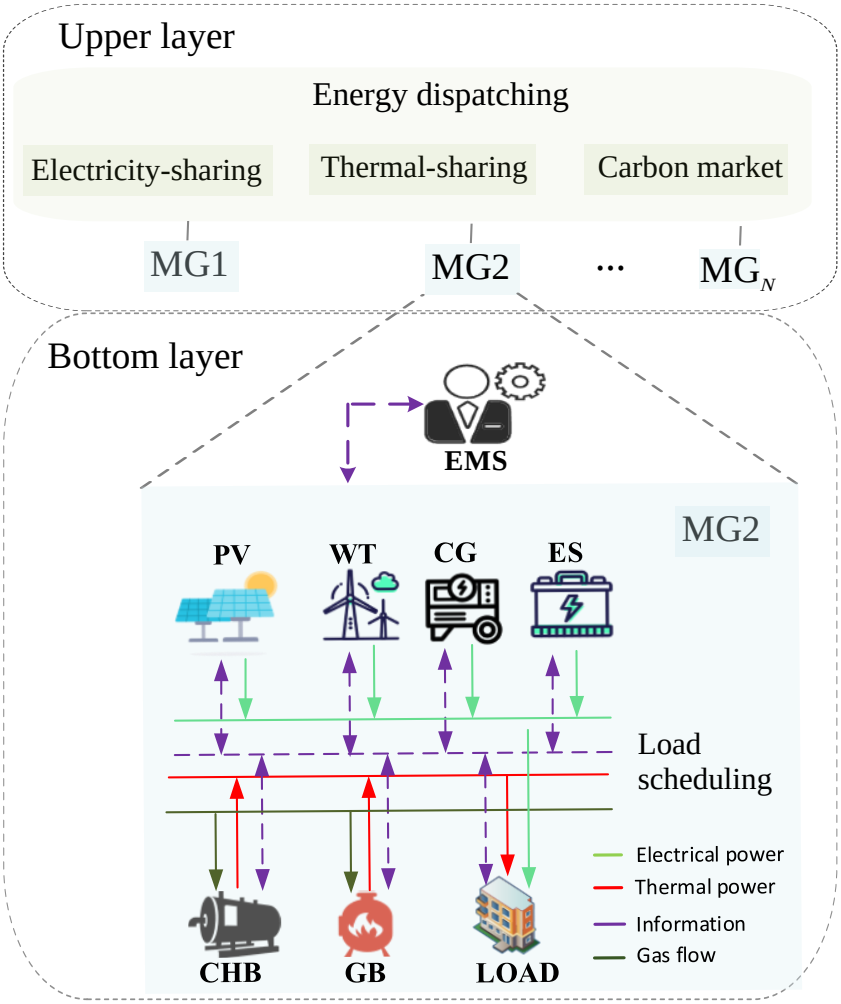

Figure 1. The structure of interconnected microgrid and energy management system. The energy management system has dual-layer optimization, including bottom-layer load scheduling and upper-layer energy dispatching.

Each MG contains three types of energy: electricity, gas, and heat. MGs include two types of load demand, namely electric and thermal loads. The energy flows are shown in Figure 2. In the energy management of the interconnected microgrids system, the scheduling range is defined in one day as $\mathcal{T} = \{1, \ldots, T\}$, where T = 24, and one hour as a time slot.

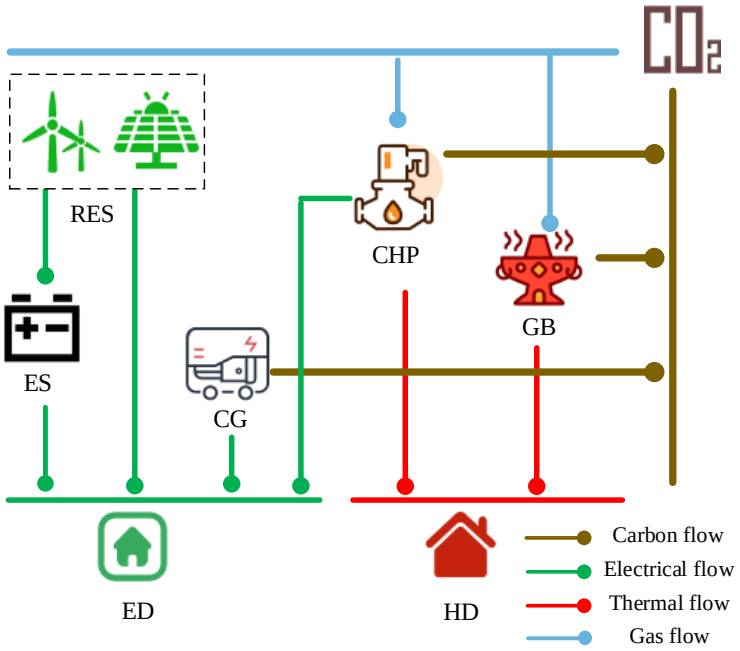

Figure 2. The energy flow of the microgrid, including electricity flow, thermal flow, carbon flow, and gas flow.

2.2. Model of Devices and Constraints

Each energy device of the interconnected microgrids system is described in detail in this section by constructing the model. The CHP model, GB model, CG model, RES model, ES model, load model, and carbon quota model are given as follows.

2.2.1. Combined Heat and Power (CHP)

The CHP is a single-input, multiple-output energy converter. It is typically characterized by high efficiency in the use of energy compared to independent sources of electricity and heat. It can produce both electric and thermal energy at the same time. The coupled thermal and electric energy for cogeneration is modeled as follows:

$$P_{i,t}^{chp} = \eta_i^{e,chp} Q_{i,t}^{chp}, \quad \forall t \in \mathcal{T}, \forall i \in \mathcal{N} \tag{1}$$

$$H_{i,t}^{chp} = \eta_i^{h,chp} Q_{i,t}^{chp}, \quad \forall t \in \mathcal{T}, \forall i \in \mathcal{N} \tag{2}$$

where $P_{i,t}^{chp}$ and $H_{i,t}^{chp}$ represent the amount of electricity generated, the amount of heat produced, and the amount of gas consumed by CHP per unit time t in microgrid i, respectively. $\eta_i^{e,chp}$ and $\eta_i^{h,chp}$ indicate the efficiency of natural gas being used by CHP to produce electricity and heat, respectively. The maximum gas consumption and ramp rate limits for CHP are given in (3) and (4).

$$0 \le Q_{i,t}^{chp} \le Q_{i,\max}^{chp}, \quad \forall t \in \mathcal{T}, \forall i \in \mathcal{N} \tag{3}$$

$$Q_i^{d,chp} \le Q_{i,t}^{chp} - Q_{i,t-1}^{chp} \le Q_i^{u,chp}, \forall t \in \mathcal{T}, \forall i \in \mathcal{N} \tag{4}$$

2.2.2. Gas Boilers (GB)

GB generates heat by burning natural gas. $\eta_i^{h,gb}$ is the heat energy conversion efficiency of the GB and $H_{i,t}^{gb}$ represents the heat production by the GB. They are described as follows:

$$H_{i,t}^{gb} = \eta_i^{h,gb} Q_{i,t}^{gb}, \quad \forall t \in \mathcal{T}, \forall i \in \mathcal{N} \tag{5}$$

In addition, the GB has a limit in the output of thermal energy, which is described by (6).

$$0 \le H_{i,t}^{gb} \le H_{i,\max}^{gb}, \quad \forall t \in \mathcal{T}, \forall i \in \mathcal{N} \tag{6}$$

2.2.3. Conventional Generators (CG)

$P_{i,t}^{cg}$ and $P_{i,\max}^{cg}$ represent the CG's power production and the maximum power production limits respectively. $P_i^{d,cg}$ and $P_i^{u,cg}$ represent the lower and upper boundaries of the slope rate of the CG respectively. They are described as follows:

$$0 \le P_{i,t}^{cg} \le P_{i,\max}^{cg}, \quad \forall t \in \mathcal{T}, \forall i \in \mathcal{N} \tag{7}$$

$$P_i^{d,cg} \le P_{i,t}^{cg} - P_{i,t-1}^{cg} \le P_i^{u,cg}, \forall t \in \mathcal{T}, \forall i \in \mathcal{N} \tag{8}$$

The fuel consumption $V_{i,t}^{cg}$, CO_2 emission $CE_{i,t}^{cg}$, and the conventional generators cost $C_{i,t}^{cg}$ are expressed as (9)–(11):

$$V_{i,t}^{cg} = \eta_i^{cg} P_{i,t}^{cg}, \quad \forall t \in \mathcal{T}, \forall i \in \mathcal{N} \tag{9}$$

where η_i^{cg} represents the fuel consumption rate, which is set to 0.24.

$$CE_{i,t}^{cg} = \alpha_{cg} P_{i,t}^{cg}, \quad \forall t \in \mathcal{T}, \forall i \in \mathcal{N} \tag{10}$$

$$C_{i,t}^{cg} = \lambda_{oil} V_{i,t}^{cg}, \quad \forall t \in \mathcal{T}, \forall i \in \mathcal{N} \tag{11}$$

where α_{cg} and λ_{oil} indicate the per unit carbon emission factor of CG and per unit price of diesel, respectively.

2.2.4. Renewable Energy (WT and PV)

WT and PV are considered to be uncontrollable generation units because of their intermittent and stochastic nature. In this paper, the historical forecast data of the microgrid are used as a relevant scenario for the experiment. $P_{i,t}^{pv}$, and $P_{i,t}^{wt}$ are the forecasted output power (in kW) of PV and wind power, respectively, which need to meet the following power limits:

$$0 \le P_{i,t}^{pv} \le P_{i,\max}^{pv}, \quad \forall t \in \mathcal{T}, \forall i \in \mathcal{N} \tag{12}$$

$$0 \le P_{i,t}^{wt} \le P_{i,\max}^{wt}, \quad \forall t \in \mathcal{T}, \forall i \in \mathcal{N} \tag{13}$$

$$P_{i,t}^{res} = P_{i,t}^{pv} + P_{i,t}^{wt}, \quad \forall t \in \mathcal{T}, \forall i \in \mathcal{N} \tag{14}$$

where $P_{i,\max}^{pv}$ and $P_{i,\max}^{wt}$ are the upper limits for the output power of PV and wind turbines, respectively. $P_{i,t}^{res}$ is the total RES output of the isolated microgrid i in per unit t (in kW).

2.2.5. Energy Storage System (ES)

The purpose of the energy storage system is to store excess electricity during low electricity consumption periods. During peak periods of electricity consumption, electricity is exported and can facilitate peak shaving and valley filling. The state of the energy storage system (ES) at time t during charging and discharging is shown in (15). $E_{i,t-1}^{s}$, $E_{i,t}^{s}$, $\eta_i^{es,c}$, and $\eta_i^{es,d}$ denote the battery state of the energy storage system at the time $t-1$ and time t, and the charging and discharging efficiency, respectively.

$$E_{i,t}^{s} = E_{i,t-1}^{s} + \eta_i^{es,c} P_{i,t}^{es,ch} \Delta t - \left(1/\eta_i^{es,d}\right) P_{i,t}^{es,dch} \Delta t \quad \forall t \in \mathcal{T}, \forall i \in \mathcal{N} \tag{15}$$

The charging and discharging power constraints are shown below:

$$0 \leq P_{i,t}^{es,ch} \leq P_{i,\max}^{es,ch} u_{i,t}^{es,ch} \tag{16}$$

$$0 \leq P_{i,t}^{es,dch} \leq P_{i,\max}^{es,dch} u_{i,t}^{es,dch} \tag{17}$$

$$0 \leq u_{i,t}^{es,ch} + u_{i,t}^{es,dch} \leq 1, \quad u_{i,t}^{es,ch}, u_{i,t}^{es,dch} \in \{0,1\} \tag{18}$$

where $P_{i,\max}^{es,ch}$ and $P_{i,\max}^{es,dch}$ are the maximum charging and discharging power of storage, respectively. The charging and discharging power are constrained in (19) according to capacity C and the binary variable $u_{i,t}^{es,ch}$, and $u_{i,t}^{es,dch}$, respectively. In particular, if u = 1, the storage is in the charged state; if $u = 0$, the storage is in the discharged or idle state. The amount of stored energy should satisfy the following constraints:

$$SOC^{es,\min} C_i^{es} \leq E_{i,t}^{es} \leq SOC^{es,\max} C_i^{es} \tag{19}$$

where C_i^{es} is the rated energy storage capacity of the energy storage unit, measured in kWh, representing the maximum energy that can be stored when the unit is fully charged. $E_{i,t}^{es}$ represents the remaining capacity of the energy storage system. Constraint (19) states the maximum SOC and the minimum SOC.

$$E_{i,1}^{es} = E_{i,24}^{es} \tag{20}$$

where $E_{i,1}^{es}$ represents the initial value of the energy storage system before the day-ahead scheduling. Typically, it may be set at around 50% of total capacity to allow for flexible charging and discharging as needed. Constraint (20) indicates that the stored energy at the beginning and end of the scheduling range should be the same.

2.2.6. Electric Loads (LOAD)

Two types of electricity loads, schedulable load and inflexible electricity load, are considered in each MG. The schedulable load can be shifted from time t to other times, while the inflexible load cannot be shifted. $P_{i,t}^{sche,in}$ and $P_{i,t}^{sche,out}$ represent the amounts of scheduled load from time t to other times. $P_{i,t}^{sche,in}$ indicates the amount of electrical load transferred in. $P_{i,t}^{sche,out}$ indicates the amount of electrical load transferred out. These loads can be calculated as follows:

$$P_{i,t}^{Oload} = P_{i,t}^{fix} + P_{i,t}^{oflex}, \quad \forall t \in \mathcal{T}, \forall i \in \mathcal{N} \tag{21}$$

$$P_{i,t,s}^{\text{sche,out}} = \rho_{i,t,s}^{out} P_{i,t}^{oflex}, \quad \forall t \in \mathcal{T}, \forall i \in \mathcal{N} \tag{22}$$

$$0 \leq \rho_{i,t,s}^{out} \leq \rho_{i,max}^{out} \tag{23}$$

$$P_{i,t,s}^{\text{sche,in}} = \rho_{i,t,s}^{in} P_{i,t}^{oflex}, \quad \forall t \in \mathcal{T}, \forall i \in \mathcal{N} \tag{24}$$

$$0 \leq \rho_{i,t,s}^{in} \leq \rho_{i,max}^{in} \tag{25}$$

where $P_{i,t}^{Oload}$ and $P_{i,t}^{oflex}$ represent the initial load and initial flex load at time slot t (in kW). $\rho_{i,t,s}^{out}$ and $\rho_{i,t,s}^{in}$ represent transfer-out and transfer-in factors. (23) and (25) represent their upper and lower bound constraints.

$$P_{i,t}^{Aflex} = P_{i,t}^{oflex} - P_{i,t,s}^{\text{sche,out}} + P_{i,t,s}^{\text{sche,in}} \tag{26}$$

The amount of electrical load transferred in should be equal to the amount of electrical load transferred out during the time range s. Then the balance constraint can be defined as follows:

$$\sum_{t\in\Phi_i^{\text{flex}}} P_{i,t,s}^{\text{sche,in}} = \sum_{t\in\Phi_i^{\text{flex}}} P_{i,t,s}^{\text{sche,out}} \tag{27}$$

The purpose of electrical load scheduling is to maximize RES utilization. The actual load of each MG changes after the electrical load shift. $P_{i,t}^{Aload}$ is the actual load after load scheduling, which is calculated as follows:

$$P_{i,t}^{Aload} = P_{i,t}^{fix} + (P_{i,t}^{oflex} - P_{i,t,s}^{\text{sche,out}} u_{i,t,s}^{out} + u_{i,t,s}^{in} P_{i,t,s}^{\text{sche,in}}) \tag{28}$$

$$\sum_{t\in\Phi_i^{\text{flex}}} \left(u_{i,t,s}^{\text{in}} + u_{i,t,s}^{\text{out}}\right) \le N_i^{\text{sche,max}} \tag{29}$$

where $u_{i,t,s}^{\text{in}}$ and $u_{i,t,s}^{\text{out}}$ denote the shifted-in and shifted-out states of the ith MG at time t of the s shifting time, respectively, as 0 and 1 variables. Φ_i^{flex} denotes the set of transferable work periods; $N_i^{\text{sche, max}}$ denotes the maximum number of transfers in the optimal cycle.

2.2.7. Carbon Quota and Carbon Trading

Carbon emission quota $W_{i,t}^{o}$ of the ith MG is calculated from (30):

$$W_{i,t}^{o} = D_{gas}\left(P_{i,t}^{chp} + P_{i,t}^{gb}\right) + D_{res} P_{i,t}^{res} \tag{30}$$

where D_{gas} represents the carbon quota associated with the production of natural gas by MG, and D_{res} denotes the carbon quota attributed to the utilization of renewable energy.

Carbon emissions come from the burning of oil by CG and the combustion of natural gas by the CHP and GB. This is expressed as in (31). em_i^{gas} and em_i^{oil} represent the CO_2 emission factors for diesel and natural gas, respectively.

$$W_{i,t}^{\text{CO}_2} = em_i^{gas}\left(Q_{i,t}^{\text{chp}} + Q_{i,t}^{\text{gb}}\right) + em_i^{oil} P_{i,t}^{cg} \tag{31}$$

The derivation of carbon trading costs for the carbon market is shown in (32):

$$C_i^{\text{CO}_2} = \sum_{t=1}^{T} \varepsilon\left(W_{i,t}^{\text{CO}_2} - W_{i,t}^{\text{o}}\right) \tag{32}$$

where ε is the carbon trading price. In the carbon trading market, the price of purchasing carbon quota is 6 YUAN/kWh and the price of selling carbon quota is 4 YUAN/kWh.

2.3. Demand–Supply Balance

Each microgrid tends to share electrical and thermal energy with other interconnected microgrids. This can reduce the operating costs of the interconnected system. Given energy production, consumption, and storage, the balance between supply and demand in the electricity and heat sectors should always be met at each time slot. The electrical power balance constraint for participation in energy sharing is the following (33):

$$P_{i,t}^{\text{cg}} + P_{i,t}^{res} + P_{t,i}^{chp} + P_{i,t}^{es,dch} = P_{i,i}^{Aload} + P_{i,t}^{es,ch} + \sum_{j\in\mathcal{N}|i} P_{i-j,t} \quad \forall t \in \mathcal{T}, \forall i \in \mathcal{N} \tag{33}$$

The heat supply and demand balance is shown in (34):

$$H_{i,t}^{h,chp} + H_{i,t}^{gb} = H_{i,t}^{Load} + \sum_{j\in\mathcal{N}|i} H_{i-j,t} \quad \forall t \in \mathcal{T}, \forall i \in \mathcal{N} \tag{34}$$

$$|P_{i-j,t}| \leq P_{i-j,\max} \tag{35}$$
$$\sum_{i \in \mathcal{N}} P_{i,t} = 0$$

$$|H_{i-j,t}| \leq H_{i-j,\max} \tag{36}$$
$$\sum_{i \in \mathcal{N}} H_{i,t} = 0$$

where $P_{i-j,t}$ and $H_{i-j,t}$ represent the amount of electrical and thermal energy shared between interconnected microgrids. (35) represents the power limit and power-sharing balance constraint on the power transmitted between the microgrids. (36) represents the heat transfer power bound and the heat sharing balance constraint.

The natural gas balance in the interconnected microgrids is described in (37):

$$Q_{i,t}^{gas} = Q_{i,t}^{chp} + Q_{i,t}^{gb}, \quad \forall t \in \mathcal{T}, \forall i \in \mathcal{N} \tag{37}$$

3. Dual-Layer Energy Management Strategy for Interconnected Microgrids

In this section, the energy management strategy is presented for the interconnected microgrids system, consisting of two layers. In the bottom layer, the gray wolf optimization algorithm is exerted to solve the electric load scheduling to achieve RES utilization. In the upper layer, the alternating direction method of the multipliers (ADMM) algorithm is utilized to optimize the energy dispatching problem. The framework of the energy management strategy for interconnected microgrid systems is shown in Figure 3.

The upper and bottom layer two objective functions are solved hierarchically. The bottom-layer objective function is addressed independently to optimize the internal load scheduling of each microgrid. Based on it, upper-layer objective function is applied to the interconnected microgrids to achieve a cost-minimized operation considering energy sharing and carbon trading. The solving of upper-layer objective function is dependent on bottom layer objective function. The upper-layer optimization relies on the outcomes of the lower-layer optimization, that is, the scheduling electric load.

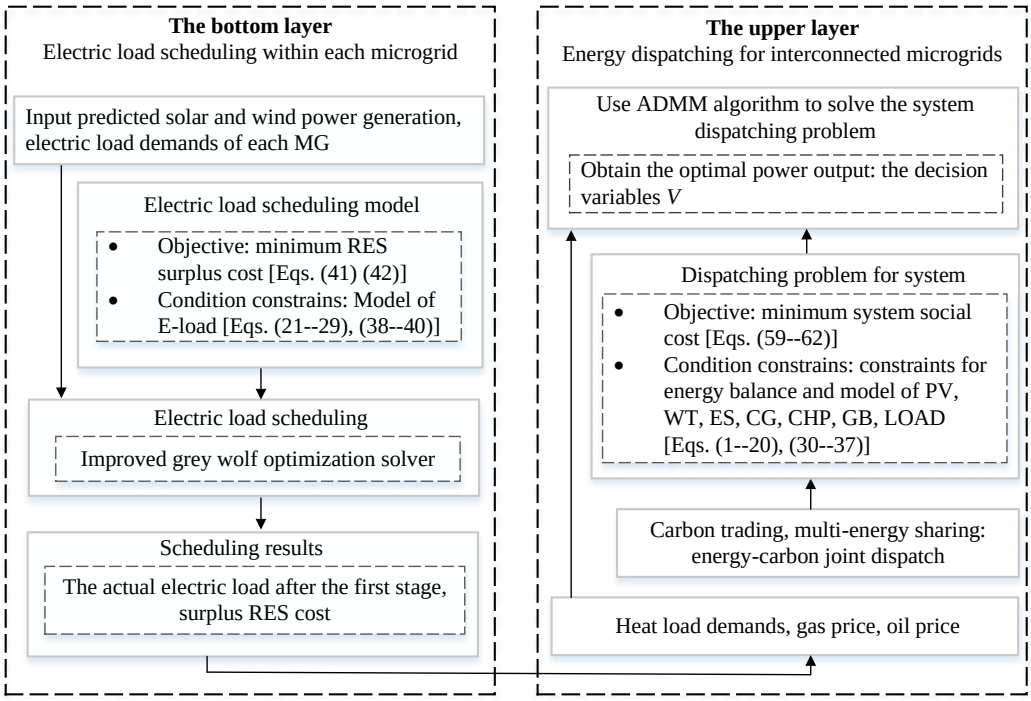

Figure 3. Dual-layer joint optimization of energy management framework consisted of load scheduling and energy dispatching for interconnected microgrids.

3.1. Electric Load Scheduling of Demand Side in Bottom Layer

The electric load scheduling can increase the utilization of renewable energy sources and thus reduce the surplus RES cost in the bottom layer of the interconnected microgrids network.

Meta-heuristic algorithms can effectively solve this class of optimization problems. Compared to other optimization algorithms such as Particle Swarm Optimization, Ant Colony Optimization, and Genetic Algorithms, the Gray Wolf Optimization algorithm stands out for its straightforward structure and simplicity in implementation. It requires the adjustment of fewer parameters, making it more accessible and efficient for solving complex optimization problems. However, the original gray wolf optimization algorithm suffers from slow convergence and the tendency to fall into local optimal solutions when solving for complex decision variables. Therefore, in this paper, a gray wolf optimization (IGWO) algorithm, improved by introducing a backward learning strategy, Cauchy variance, and the nonlinear convergence factor, is proposed to overcome the above problems.

3.1.1. Problem Description and Objective Function

The initial surplus renewable energy is defined as follows [32]:

$$P_{sys,t}^{sur} = \sum_{i=1}^{N} P_{i,t}^{res} - \sum_{i=1}^{N} P_{i,t}^{Oload} \tag{38}$$

When the transfer optimization of the electric load is carried out, the actual electric load at each moment t is follows:

$$\begin{aligned} P_{i,t}^{Aload} &= P_{i,t}^{Oload} - P_{i,t,s}^{\text{sche,out}} + P_{i,t,s}^{\text{sche,in}} \\ &= \left(1 - \rho_{i,t,s}^{out} + \rho_{i,t,s}^{in}\right) P_{i,t}^{Oload} \end{aligned} \tag{39}$$

where $P_{i,t}^{Aload}$ and $P_{i,t}^{Oload}$ denote the actual electrical load after the bottom layer scheduling and the initial electrical load, respectively. $P_{i,t,s}^{\text{sche,out}}$ and $P_{i,t,s}^{\text{sche,in}}$ represent the electrical power of the i th microgrid scheduled in or out at time slot t. $\rho_{i,t,s}^{out}$ and $\rho_{i,t,s}^{in}$ represent the transfer in or out factor, respectively.

At the same time, we define the actual surplus renewable energy as follows:

$$P_{sys,t}^{Asur} = \sum_{i=1}^{N} P_{i,t}^{res} - \sum_{i=1}^{N} P_{i,t}^{Aload} \tag{40}$$

The optimization objective of the bottom-layer load scheduling is to maximize the utilization of RES and minimize user dissatisfaction and surplus RES cost. Therefore, the objective function for the bottom layer is as follows:

$$\begin{aligned} minf1 = minC_{BottomLayer} &= \sum_{t=1}^{T} C_{sys,t}^{res} + \sum_{t=1}^{T} C_{sys,t}^{\text{dissatisfaction}} \\ &= \sum_{t=1}^{T} C_{sys,t}^{res} + \sum_{t \in \Phi_i^{\text{flex}}} \lambda_{dis} (P_{i,t}^{Oload} - P_{i,t}^{Aload} \Delta(t))^2 \\ &= \sum_{t=1}^{T} \lambda_{sur} P_{sys,t}^{\text{Asur}} + \sum_{t \in \Phi_i^{\text{flex}}} \lambda_{dis} (P_{i,t}^{Oload} - P_{i,t}^{Aload} \Delta(t))^2 \end{aligned} \tag{41}$$

$$P_{sys,t}^{\text{Asur}} = \begin{cases} \sum_{i=1}^{N} P_{i,t}^{res} - \sum_{i=1}^{N} P_{i,t}^{Aload}, \sum_{i=1}^{N} P_{i,t}^{RES} > \sum_{i=1}^{N} P_{i,t}^{Oload} \\ 0, \sum_{i=1}^{N} P_{i,t}^{res} \leq \sum_{i=1}^{N} P_{i,t}^{Oload}. \end{cases} \tag{42}$$

In (41), λ_{dis} is the weight coefficient for user dissatisfaction cost, which represents the dissatisfaction factor of the difference between the initial load and the actual load after the load transfer. λ_{sur} represents the surplus price for RES, with the unit cost of the remaining renewable energy set to 2.5 YUAN/kWh.

3.1.2. The IGWO Algorithm for Electric Load Scheduling

The gray wolf optimization algorithm simulates the characteristics of a gray wolf pack during the pack hierarchy [33], by constantly searching and pursuing the prey, constantly updating the location of the prey, and finally successfully hunting [34]. In the gray wolf optimization algorithm, wolves are divided into α wolf, β wolf, δ wolf, and the rest of the individual wolves ω in descending order of rank [35].

The α wolf is the leader wolf and plays a leadership and decision-making role in the pack. The β wolf is a leader candidate and feeds information to the α wolf in the pack. The δ wolf is responsible for the leadership of the ω wolf pack; the ω wolf searches for and pursues its prey. The gray wolf obtains its prey in three steps:

S1: Surrounding the prey. The action of a gray wolf encircling its prey can be described as follows [14]:

$$D = \left| \boldsymbol{C} \cdot \boldsymbol{X}_{\mathrm{p}}(l) - \boldsymbol{X}(l) \right| \tag{43}$$

$$\boldsymbol{X}(l+1) = \boldsymbol{X}_{\mathrm{p}}(l) - \boldsymbol{A} \cdot D \tag{44}$$

$$\boldsymbol{A} = 2a \cdot \boldsymbol{r}_1 - a \tag{45}$$

$$\boldsymbol{C} = 2\boldsymbol{r}_2 \tag{46}$$

(43) represents the distance between the gray wolf and its prey; (44) is the action for updating the position of the gray wolf. $\boldsymbol{X}_{\mathrm{p}}(l)$ is the position of the prey at iteration l; $\boldsymbol{X}(l)$ is the position of the gray wolf at iteration l, and $X(l+1)$ is the position of the gray wolf at the next iteration. $\boldsymbol{C}$, $\boldsymbol{A}$ are the coefficient vectors; a is the convergence factor, linearly decreasing from 2 to 0; l is the number of current iterations; $\boldsymbol{r}_1$, $\boldsymbol{r}_2$ are random parameters between $[0, 1]$.

A backward learning strategy is proposed to improve the original gray wolf optimization. In the original algorithm, the populations generated by the stochastic strategy do not exploit the spatial information well enough. Therefore, the convergence speed is unpredictable and the computation consumes much time. The main idea of the inverse learning strategy is to increase the diversity of the population and increase the probability of obtaining a better solution by searching the positive and negative directions of the space. The calculation of the inverse solution is as follows [36]:

$$X_{i+1}(l)' = rand(u_b + l_b) - X_{i+1}(l) \tag{47}$$

where $X_{i+1}(l)$ denotes the position of the $(i+1)$th wolf in the solution space, $X_{i+1}(l)'$ denotes the inverse solution of $X_{i+1}(l)$; $rand$ is a random number, randomly taken at $[0, 1]$; u_b and l_b represent the upper and lower bounds of the positions, respectively. After obtaining the inverse solution, the better position can be selected from the original solution and the inverse solution can be selected as the initial position of the next iteration.

In the original gray wolf optimization algorithm, the size of coefficient vector A determines whether the gray wolf is globally searched or locally exploited, and it varies with the convergence factor a. The linear variation h leads to a local optimum situation, which is an obstacle to performing a global search. In interconnected microgrid load scheduling, changing factor a from 2 linearly decreasing to 0 is difficult to adapt to the actual situation, because this optimization problem is not a linear convergence problem. For the algorithm to better balance the global and local search ability, a new formulation is

proposed in this paper. The convergence factor a decreases nonlinearly with the number of iterations, and the specific expression is as follows:

$$a = (a_{\max} - a_{\min}) \cos\left(\frac{1}{2w}\left(\frac{l}{L_{\max}}\right)^{\lambda} \times \pi\right) \tag{48}$$

where $a_{\max}$ indicates the maximum value of convergence factor 2; $a_{\min}$ is the minimum value of convergence factor 0; l is the number of d current iterations; L_{max} denotes the maximum number of iterations. w and λ are the adjustment parameters. It can be seen that the original slope is constant and decreases linearly, while the improved one maintains a larger value slowly decreasing at the initial stage, and the reduced decay rate is more conducive to the global search for the optimal solution. The later period increases its decay rate, which can search the local optimal solution more accurately. This improvement can ensure the exploration and development capability of the algorithm, which can balance the performance of global search and local development.

S2: Hunting for prey.

The distances between α, β, and δ wolves and their prey during predation are calculated by (49)–(51). ω wolves approach their prey based on the position of α wolf, β wolf, and δ wolf. The direction and step length of ω wolves towards α wolf, β wolf, and δ wolf, respectively, can be calculated from (52) to (54):

$$D_{\alpha} = |C_1 \boldsymbol{X}_{\alpha} - \boldsymbol{X}_{\omega}| \tag{49}$$

$$D_{\beta} = \left|C_2 X_{\beta} - X_{\omega}\right| \tag{50}$$

$$D_{\delta} = |\boldsymbol{C}_3 \boldsymbol{X}_{\delta} - \boldsymbol{X}_{\omega}| \tag{51}$$

$$\boldsymbol{X}_1 = \boldsymbol{X}_{\alpha} - \boldsymbol{A}_1 D_{\alpha} \tag{52}$$

$$X_2 = \boldsymbol{X}_{\beta} - \boldsymbol{A}_2 D_{\beta} \tag{53}$$

$$\boldsymbol{X}_3 = \boldsymbol{X}_{\delta} - \boldsymbol{A}_3 D_{\delta} \tag{54}$$

The final position of the ω wolf is as follows:

$$\boldsymbol{X}_{\omega}(l+1) = \frac{\boldsymbol{X}_1 + \boldsymbol{X}_2 + \boldsymbol{X}_3}{3} \tag{55}$$

where D_{α}, D_{β}, and D_{δ} are the distances between the α, β, δ wolves, and ω wolves, respectively; X_{α}, X_{β}, and V_{δ} are the positions of α, β and δ wolf, respectively; X is the position of ω wolf and $X(l+1)$ is the final position of the next ω wolf.

The original algorithm is improved by introducing a Cauchy variant. Cauchy variation is applied to the locations of gray wolves. The variation operation selects individuals from wolves α, β, and δ and mutates their locations, thus expanding the population size to obtain more random positions. This can enhance the ability of the algorithm to go beyond the local optimum to search for a better solution. The formula of the Cauchy mutation for the leading wolf individual is as follows:

$$X_{\alpha new} = X_{\alpha} + X_{\alpha} \cdot \text{ Cauchy } (0,1) \tag{56}$$

$$X_{\beta new} = X_{\beta} + X_{\beta} \cdot \text{ Cauchy } (0,1) \tag{57}$$

$$X_{\delta new} = X_{\delta} + X_{\delta} \cdot \text{ Cauchy } (0,1) \tag{58}$$

where Cauchy $(0,1)$ denotes the standard Cauchy function, X_{α}, X_{β}, and X_{δ} are the current solution, and $X_{\delta new}$, $X_{\beta new}$, and $X_{\alpha new}$ are the solutions after Cauchy variation. From (56) to (58), it can be seen that the Cauchy variation of the solution is equivalent to a local search around the optimal solution. The new solution generated by (56)–(58) is not necessarily better than the original solution. Therefore, in the calculation, if the new solution has a better fitness value, the original solution is replaced; otherwise, it remains unchanged.

S3: Attacking the prey.

When the prey stops moving, the gray wolf completes the hunt by attacking. Or, as the value of the approximation a to the prey gradually decreases, the corresponding $|A|$ varies within $[-a, a]$. When $|A| < 1$, the algorithm converges and the prey position is obtained.

3.2. Energy Dispatching with Energy Sharing and Carbon Trading in Upper Layer

The microgrids are connected to achieve their own and global cost optimization by sharing multi-energy. Centralized optimization approaches require complete information about each microgrid, which can lead to communication jams and microgrid privacy risks. Therefore, in this paper, a distributed algorithm is developed for energy optimization dispatch based on the alternating direction method of multipliers.

3.2.1. Problem Description and Objective Function

Based on the forecasted values of renewable energy generation and electrical and thermal loads, the objective of the energy dispatching is to minimize the social operating costs and carbon emissions of the interconnected microgrids. To make full use of renewable energy, the curtailment cost for RES is introduced. The objective function and constraints of the interconnected microgrids network are as follows:

$$\begin{aligned} minf2 &= \min C_{UpperLayer} \\ &= \sum_{i=1}^{N}\sum_{t=1}^{T}\left(C_{i,t}^{cg} + C_{i,t}^{gas} + C_{i,t}^{cutRES}\right) \\ &+ \sum_{i=1}^{N} C_{i}^{CO_2} + C_{BottomLayer} \end{aligned} \tag{59}$$

$$C_{i,t}^{\mathrm{cg}} = \lambda_{oil} V_{i,t}^{\mathrm{cg}} \tag{60}$$

$$C_{i,t}^{\mathrm{gas}} = \lambda_{gas} Q_{i,t}^{\mathrm{gas}} \tag{61}$$

$$C_{i,t}^{cutRES} = \lambda_{i}^{cut} P_{i,t}^{curtRES} \tag{62}$$

The total cost is the sum of CG fuel cost, gas cost, renewable energy curt cost, carbon trading cost, and electricity load optimization costs, as shown by (60)–(62). λ_{oil}, λ_{e}^{gas}, and λ_{i}^{cut} denote the diesel price, gas price, and RES shedding penalty price, respectively. $C_{BottomLayer}$ is the optimized value achieved through the internal load scheduling within each microgrid by (41), and is incorporated into (59). The decision variables are $V = \left\{P_{i,t}^{chp}, H_{i,t}^{chp}, P_{i,t}^{cg}, P_{i,t}^{pv}, P_{i,t}^{wt}, H_{i,t}^{gb}, P_{i,t}^{es,ch}, P_{i,t}^{es,dch}, u_{i,t}^{es,ch}, u_{i,t}^{es,dch}, P_{i-j,t}, H_{i-j,t}\right\}$.

3.2.2. The ADMM Algorithm for Energy Dispatching Strategy

As the energy sharing balance constraints are multiply coupled between all microgrids, the auxiliary variables $P_{j-i,t}$ and $H_{j-i,t}$ are introduced. A double coupling model is developed:

$$\begin{aligned} P_{j-i,t} + P_{i-j,t} &= 0 \\ H_{j-i,t} + H_{i-j,t} &= 0 \end{aligned} \tag{63}$$

The model has multi-coupling variables. In (63), $P_{i-j,t}$ indicates that the amount of electricity MG i expects to share with MG j. $P_{j-i,t}$ indicates that the amount of electricity MG j expects to share with MG i. $H_{i-j,t}$ indicates that the amount of thermal energy MG i expects to share with MG j. $H_{j-i,t}$ indicates that the amount of thermal energy MG j expects to share with MG i. When $P_{i-j,t} = -P_{j-i,t}$ and $H_{i-j,t} = -H_{j-i,t}$, it indicates that the energy-sharing consensus is reached between MG i and MG j.

The optimal solution to the problem (59) can be achieved by iterating the original objective function decision variables V, Lagrange multipliers, and auxiliary variables

alternatively. After completing the decoupling transformation, the specific steps of the distributed solution based on the alternating direction method of multipliers (ADMM) algorithm are as follows: The initial energy dispatching problem is a scheduling problem presented in (59).

step 1: Construct an extended Lagrangian function.

The original optimization problem $minf$ in which f contains the decision variable V. f is defined as $f_i(x_i, t)$, where i represents the ith MG, and x_i denotes the optimal variables, and t indicates scheduling timescale one hour. Therefore, the Lagrangian function for the problem (59) is established as follows:

$$\begin{aligned} L_{\rho_i^{\mathrm{H}},\rho_i^{\mathrm{P}}}(P_{j-i}, H_{j-i}, \lambda_{i,t}^{\mathrm{P}}, \lambda_{i,t}^{\mathrm{H}}) = C_{UpperLayer} + \\ \sum_{j}^{\mathcal{I}} \sum_{t=1}^{T} \lambda_{i-j,t}^{\mathrm{P}} \left(P_{i-j,t} + P_{j-i,t}\right) + \\ \sum_{j}^{\mathcal{I}} \sum_{t=1}^{T} \lambda_{i-j,t}^{\mathrm{H}} \left(H_{i-j,t} + H_{j-i,t}\right) + \\ \sum_{j}^{\mathcal{I}} \frac{\rho_i^{\mathrm{P}}}{2} \sum_{t=1}^{T} \left\| P_{i-j,t} + P_{j-i,t} \right\|_2^2 + \\ \sum_{j}^{\mathcal{I}} \frac{\rho_i^{\mathrm{H}}}{2} \sum_{t=1}^{T} \left\| H_{i-j,t} + H_{j-i,t} \right\|_2^2 \end{aligned} \tag{64}$$

In (64), the λ is the Lagrange multiplier and ρ is the penalty parameter.

step 2: Update auxiliary and optimization variables.

Each MG updates its energy-sharing policy via local computing between MGs, and only information about energy sharing is exchanged between MGs. Let k denote the number of iterations. MG i updates its decision $P_{j-i,t}(k+1)$ and $H_{j-i,t}(k+1)$ according to (65) and (66).

$$\begin{cases} P_{i-j,t}(k+1) = \arg\min L_i\left(\lambda_{i-j}(k), P_{i-j,t}(k), P_{j-i,t}(k)\right) \\ H_{i-j,t}(k+1) = \arg\min L_i\left(\lambda_{i-j}(k), H_{i-j,t}(k), H_{j-i,t}(k)\right) \end{cases} \tag{65}$$

$$\begin{cases} P_{j-i,t}(k+1) = \arg\min L_i\left(\lambda_{i-j}(k), P_{i-j,t}(k+1), P_{j-i,t}(k)\right) \\ H_{j-i,t}(k+1) = \arg\min L_i\left(\lambda_{i-j}(k), H_{i-j,t}(k+1), H_{j-i,t}(k)\right) \end{cases} \tag{66}$$

According to the update rules above, the optimization variables as well as the auxiliary variables in the original problem can be solved for each iteration.

step 3: Update the Lagrange multiplier.

The Lagrange multiplier is updated according to (67).

$$\begin{aligned} \lambda_{i-j,t}^{P}(k+1) &= \lambda_{i-j,t}^{P}(k) + \rho_{i,t}^{P}\left(P_{i-j}(k+1) + P_{j-i}(k+1)\right) \\ \lambda_{i-j,t}^{H}(k+1) &= \lambda_{i-j,t}^{H}(k) + \rho_{i,t}^{H}\left(H_{i-j}(k+1) + H_{j-i}(k+1)\right) \end{aligned} \tag{67}$$

The three steps repeat sequentially until the following stop condition (68) is met:

$$\begin{aligned} \sum_{t=1}^{T} \sum_{i=1}^{\mathcal{I}} \left\| P_{i-j,t}(k+1) - P_{i-j,t}(k) \right\|_2^2 \le \epsilon_1 \\ \sum_{t=1}^{T} \sum_{i=1}^{\mathcal{I}} \left\| H_{i-j,t}(k+1) - H_{i-j,t}(k) \right\|_2^2 \le \epsilon_2 \end{aligned} \tag{68}$$

where ϵ_1 and ϵ_2 are sufficient small values. Note that the left-hand side of (68) represents the raw residuals of the distributed algorithm.

Following the above iterative steps, the power optimization of each MG is completely decoupled and can be solved independently. The information transfer during the solution process occurs only between neighboring MGs without any global information interaction, which greatly reduces the communication cost. In addition, the communication does not involve the internal operation state of each MG, which can effectively protect privacy.

4. Numerical Simulation and Analysis

For interconnected microgrids consisting of three microgrids (MG1, MG2, MG3), the energy optimization simulation of multiple microgrids is validated in this section. The proposed dual-layer energy management strategy is well evaluated in the simulation. In this case, each microgrid has a similar structure but a different energy composition. The sharing of electrical and thermal energy between microgrids is considered. This can increase the viability of the system and reduce the social operation cost. Specifically, the energy cost unit in this paper is converted into the RMB unit, YUAN.

The parameters of ES for each microgrid energy device and the parameters of CGs, CHPs, and GBs are shown in Table 1. By participating in transactions, each microgrid has the capacity to sell its surplus renewable energy to other microgrids. Conversely, if a microgrid experiences a deficit in energy, this demand will incentivize it to engage in energy trading to meet its needs. We consider the utilization of renewable energy and the unit cost of the remaining renewable energy to be 2.5 YUAN/kWh. The price of natural gas at the national gas plant is fixed at 2.2 YUAN/kWh at all time instants, and the price of diesel fuel burned by conventional power generation equipment is 7 YUAN/kWh [37]. The convergence accuracy of the optimization algorithm is predefined as 0.1 kW.

Table 1. Parameters of interconnected microgrids system controllable equipment.

Equipments	Capacity	Parameters
CHP	$P_{i,\max}^{chp} = 1000$ kW, $Q_{i,\max}^{chp} = 500$ kW	$\eta_i^{e,chp} = 0.6, \eta_i^{h,chp} = 0.8$
GB	$Q_{i,\max}^{gb} = 600$ kW	$\eta_i^{h,gb} = 0.9$
ES	$E^s = 500$ KW, $P_{i,max}^{es,ch}, P_{i,max}^{es,dch} = 400$ kW, $P_{i,min}^{es,ch}, P_{i,min}^{es,dch} = 100$ kW	$\eta_i^{es,c} = 0.93, \eta_i^{es,d} = 0.95$
CG	$P_{i,\max}^{CG} = 800$ kW	$\eta_i^{cg} = 0.24$

To reduce carbon emission, carbon trading is introduced for the interconnected microgrids in this paper. The carbon trading is not conducted for free but occurs within a market framework where a trading price is established. The unit cost of carbon emission, carbon emission factors, and carbon quota of three MGs are given in Table 2 [37]. In the carbon trading market, the price of the purchasing carbon quota is 6 YUAN/kWh and the price of the selling carbon quota is 4 YUAN/kWh. Meanwhile, the parameters of the dual-layer algorithm are shown in Table 3.

Table 2. Carbon trading parameters of interconnected microgrids system, including the carbon quota and emission rate of gas and CG.

MG	Gas Quota	Rate	CG Quota	Rate	Res Quota
MG1	0.233	0.19	0.71	1.07	0.094
MG2	0.234	0.20	0.72	1.07	0.093
MG3	0.232	0.21	0.73	1.17	0.095

Table 3. Algorithm parameter settings.

ADMM	Parameter
Maximum iterations	500
Tolerant	0.01
Rho e	1×10^{-3}
Rho h	1×10^{-3}
Iterations	1000
Population size	500

4.1. Raw Data

The predicted output data of PV and WT of the microgrid for the three islands are given in Figure 4a,b, respectively. The data of PV and WT of the microgrid for the three islands are described in [38,39] and shown in Figure 4a,b, respectively. The electrical and thermal loads reported in [40] are utilized, as shown in Figure 4c,d. For realizing the day-ahead scheduling, LSTM network [41] is utilized to predict the renewable energy and user load for the following day based on the historical data in dataset. To reduce carbon emissions, natural gas consumption is given priority, and diesel consumption is selected later. The price of natural gas from national gas plants is fixed at 2.2 YUAN/kWh for all periods [42]. The price of diesel fuel burned by CG is 7 YUAN/kWh [43].

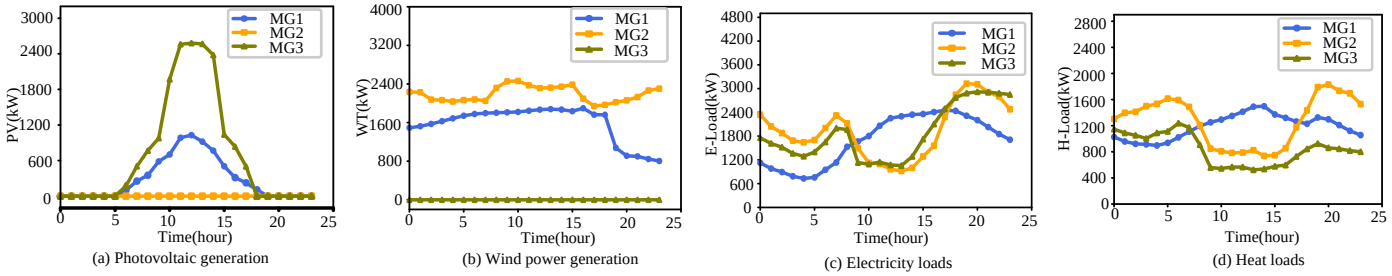

Figure 4. Photovoltaic, wind power generation, electric loads, and heat loads of the three microgrids.

4.2. The Analysis of Load Scheduling Using IGWO

The comparative area of RES and load of interconnected microgrids system before and after the load scheduling is shown in Figure 5. From this figure, it can be seen that after load scheduling, the interconnected microgrids system can consume a portion of RES to the maximum extent and improve the utilization of renewable energy. The convergence result of the improved gray wolf algorithm is presented in Figure 6. The improved gray wolf algorithm converges faster and has a smaller fitness value than the original algorithm. It can be seen that in the bottom layer, the surplus RES cost after load scheduling by the improved gray wolf algorithm is 11,291.67 YUAN. Figure 7 shows the comparison of the renewable energy surplus before and after load scheduling for each microgrid. The "before" refers to the operational outcomes of the system without employing the scheduling algorithm presented in this paper, and the system operation is generally rule-based [44]. It can be seen that the remaining renewable energy for each MG decreases to a large extent. The RES utilization rate before load scheduling is 74.2%, and the RES utilization rate after load scheduling is 91.6%. Therefore, it can be seen from the simulation results that the maximum RES utilization algorithm based on the improved gray wolf optimization algorithm (IGWO) can overcome the deficiency of insufficient RES utilization.

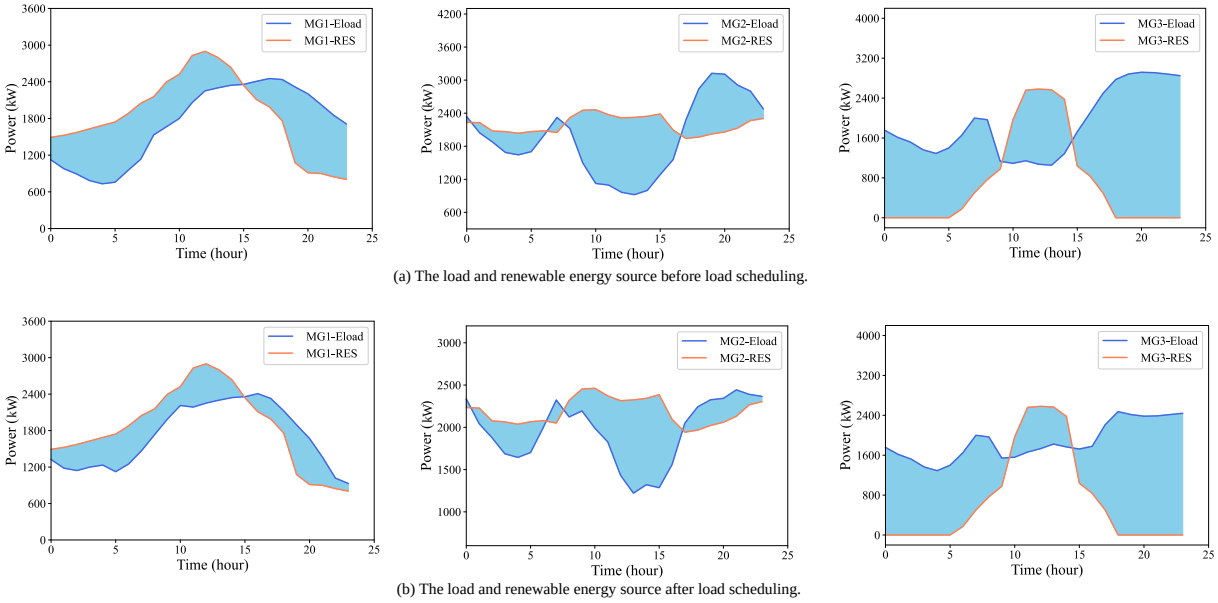

Figure 5. Comparison of renewable energy utilization before and after load scheduling. (**a**) The load and renewable energy source before load scheduling; (**b**) the load and renewable energy source after load scheduling.

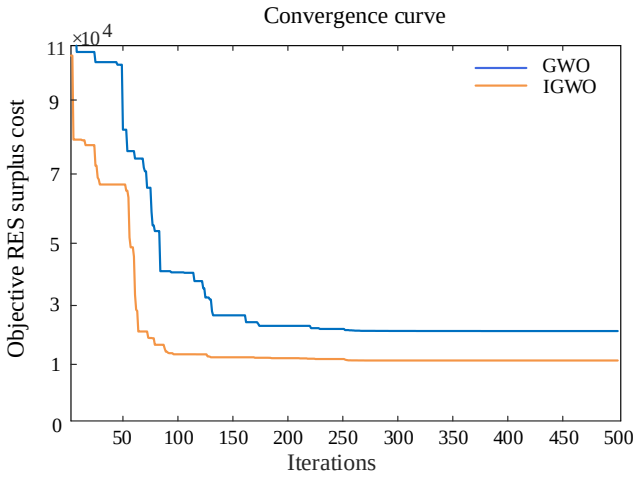

Figure 6. Comparison of convergence curves of the original gray wolf algorithm and the improved gray wolf algorithm for load scheduling after 500 iteration rounds.

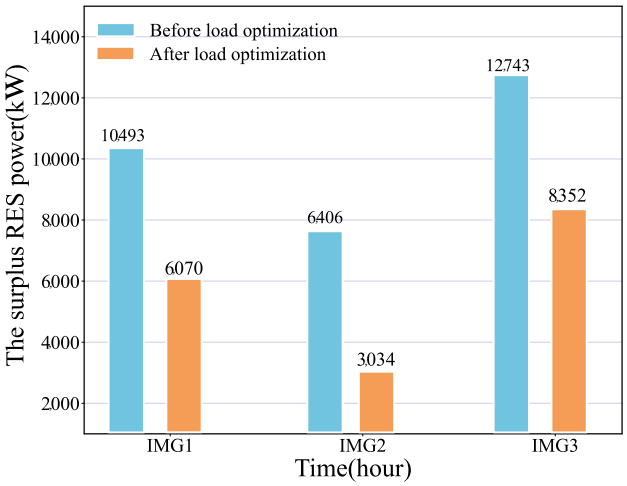

Figure 7. The total residual RES before and after the load scheduling of the MGs.

4.3. Energy Dispatching Results Using ADMM

In the stopping condition (68), the residuals are set to 0.001 and 0.01. We verify the convergence performance of the alternating direction method of the multipliers-based distributed algorithm. As shown in Figure 8, the convergence process and operation cost of the interconnected microgrids are shown based on the distributed algorithm of the alternating direction method of multipliers. Figure 8 illustrates the variation in f2 cost during the iterative optimization process. Because the solving iterations are not coupled between bottom optimization and top optimization layer, there are different tendencies between Figures 6 and 8. Figure 8 shows that the iterative convergence cost of MG1 is 6.0908 YUAN and the iterative convergence cost of MG2 is 7.1234 YUAN. The iterative convergence cost of MG3 is 8.2136 YUAN. The coalition of interconnected microgrids energy scheduling based on the ADMM distributed algorithm can converge to the optimal value of 20.8950 YUAN after about the 30th iteration. This indicates a relatively fast convergence of the algorithm. At the same time, these results demonstrate the effectiveness of the proposed distributed algorithm in solving the interconnected microgrid energy dispatching problem.

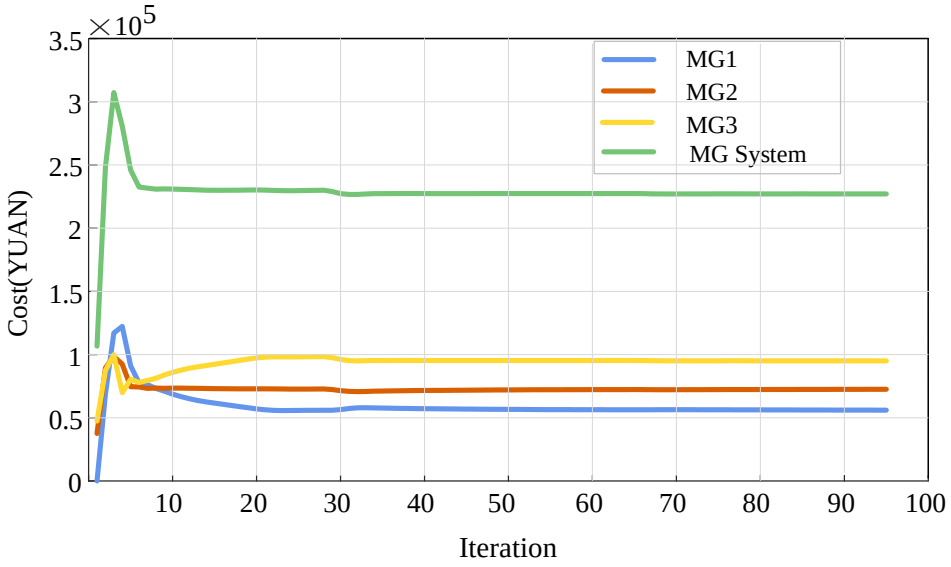

Figure 8. Convergence curves of running cost per MG and social running cost of the interconnected microgrids system.

4.4. Multi-Energy Sharing Results

The result of electric energy sharing is shown in Figure 9, and the result of thermal energy sharing is shown in Figure 10. From the resulting figures, we can find that the energy shared by electric energy and thermal energy is balanced at each time slot t (1 h). The alliance between microgrids for multi-energy sharing can solve the problem of the weak viability of individual MGs. All MGs are on islands and disconnected from the main grid. To meet the supply–demand balance of the system and to achieve economic efficiency, energy is shared among the three MGs through internal coordination.

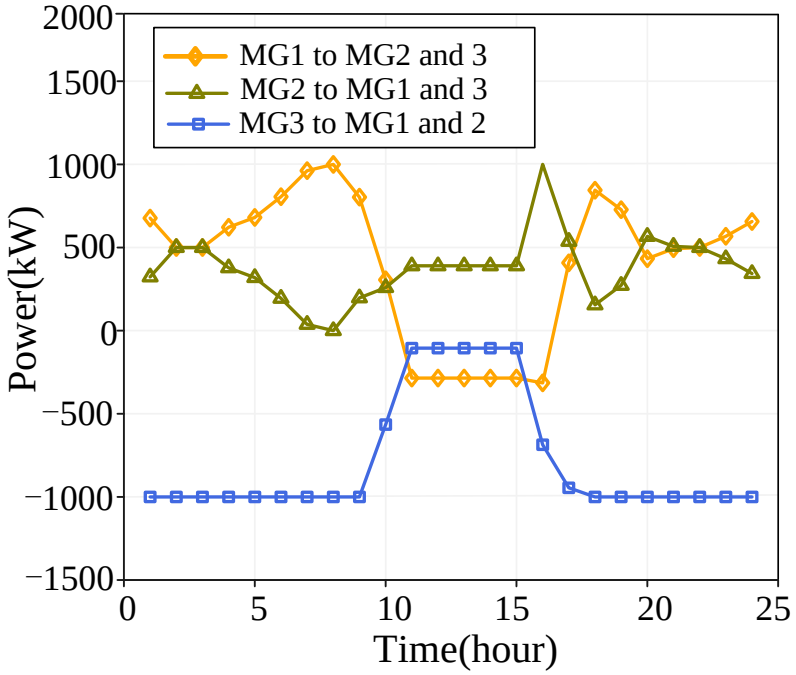

Figure 9. The electricity power sharing between interconnected microgrids.

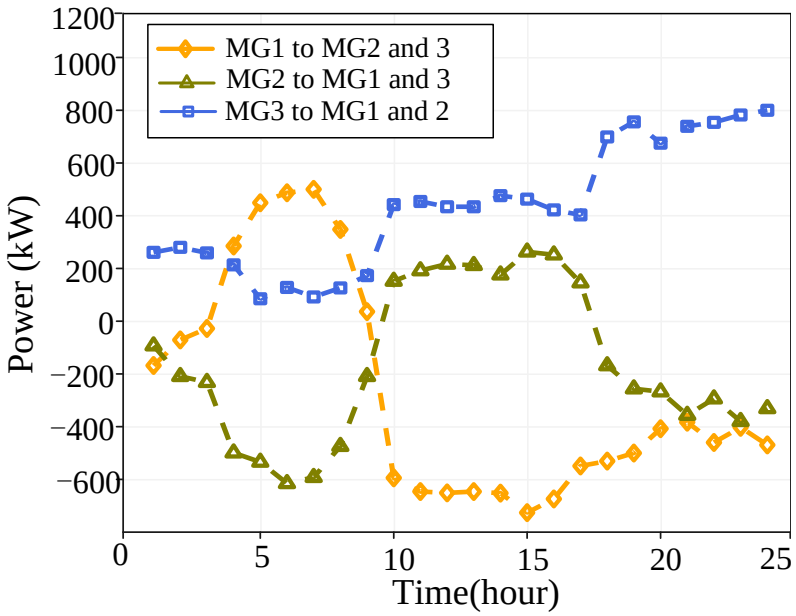

Figure 10. The thermal power sharing between interconnected microgrids.

The energy dispatching results for each microgrid are shown in Figures 11 and 12. The power dispatch results for the power outputs of CG, CHP, ES, PV, and WT of MG1, MG2, and MG3 are shown in Figure 11. In Figure 12, the thermal power dispatch results for the power output of CHP, GB, and thermal energy sharing of MG1, MG2, and MG3 are shown. The power output of thermal energy mainly comes from CHP and GB and thermal energy sharing from other microgrids. The power output of electricity is mainly from renewable energy, CHP, and CG. Analyzing the dispatch results, it can be seen that the CGs of MG1 and MG2 do not produce power. Only the CG of MG3 output power in the evening hours. This is because the price of diesel required for CG power generation is higher than the price of natural gas for gas-based equipment and the microgrid prefers to use natural gas equipment for electricity generation.

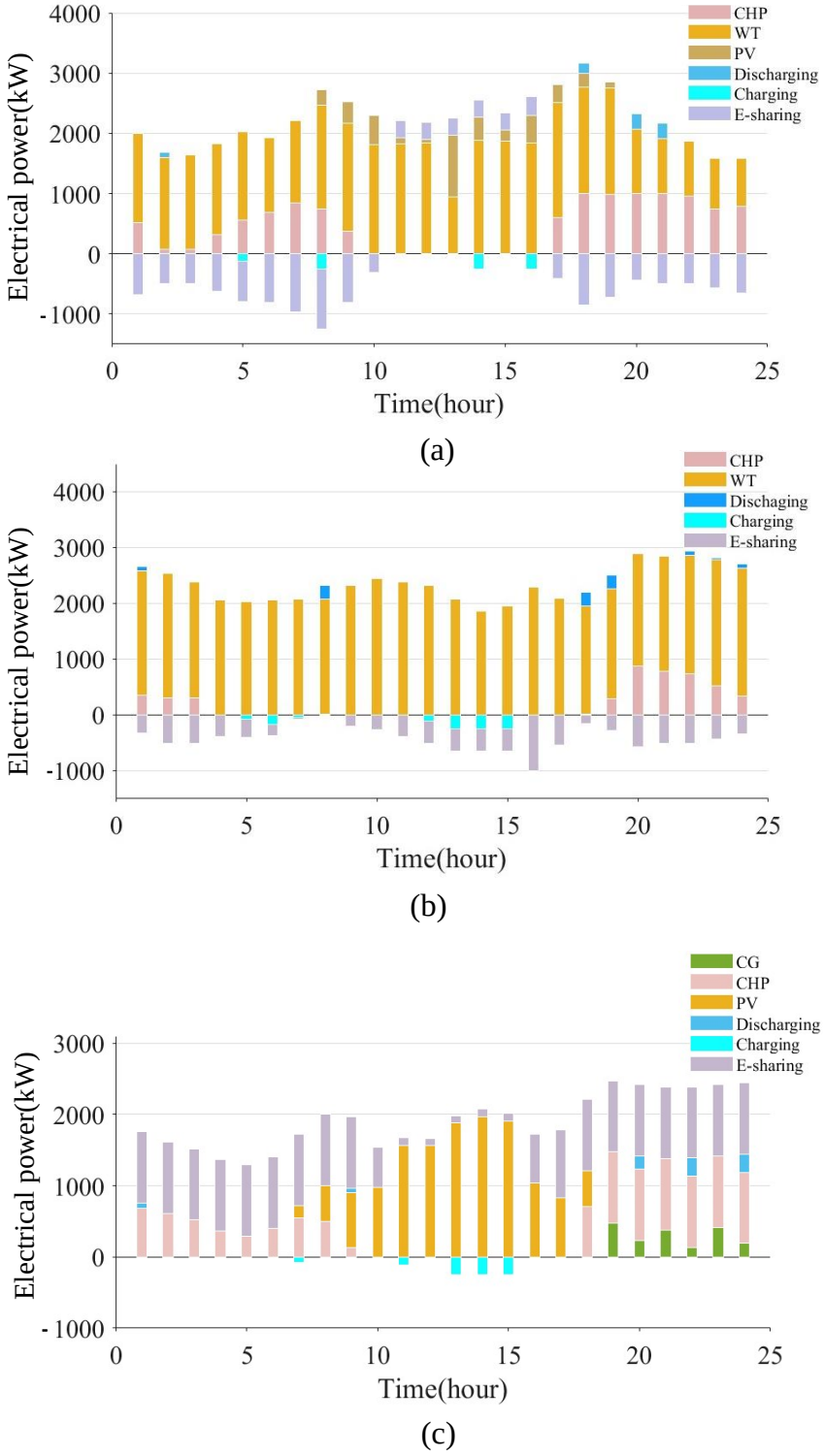

Figure 11. Electricity dispatching results of the three microgrids, including the electrical power output of renewable energy sources (PV, WT), combined heat and power units (CHP), conventional generators (CG), the charging and discharging of energy storage systems (ES), and electricity sharing in time slot *t*. (**a**) The results of MG1; (**b**) the results of MG2; (**c**) the results of MG3.

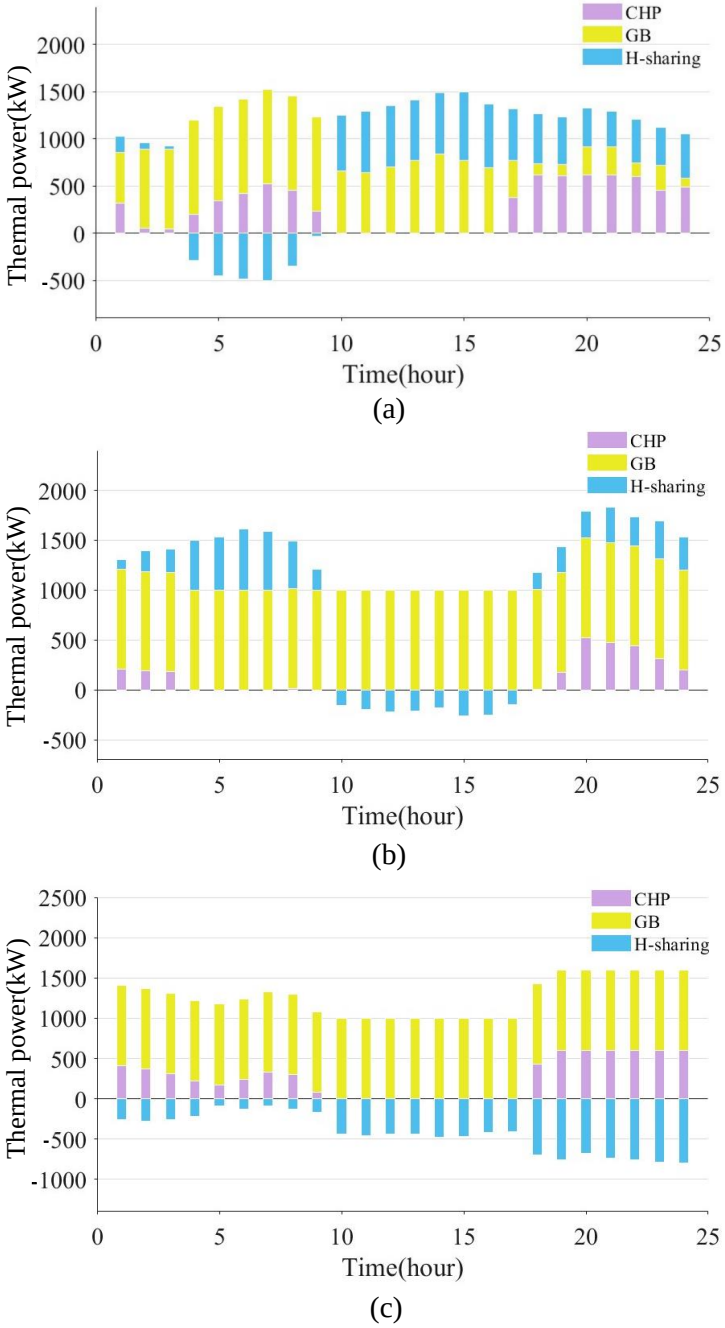

Figure 12. Thermal dispatching results of these three microgrids, including the thermal power output of combined heat and power units (CHP), gas boilers (GB), and thermal sharing in time slot t. (**a**) the results of MG1; (**b**) the results of MG2; (**c**) the results of MG3.

4.5. Comparison of Dispatching Results Under Different Scenarios

Four different scheduling methods are considered to analyze the performance of the proposed energy management strategy:

Method 1: No electric load scheduling of demand side and electricity–thermal energy sharing among microgrids.

Method 2: Electric load scheduling of demand side and no electricity–thermal energy sharing among microgrids.

Method 3: Electricity–thermal energy sharing without considering electric load scheduling of demand side among microgrids.

Proposed method: Electric load scheduling of demand side and electricity–thermal energy sharing among microgrids.

The comparison of renewable energy abandonment, carbon emission, and social cost for the three scenarios is presented in Table 4. It can be seen that the carbon emission, social cost, and renewable energy abandonment are the lowest for the dual-layer renewable energy utilization and multi-energy dispatching joint optimization strategy proposed in this paper.

Table 4. Comparison of different dispatching methods: Method 1, Method 2, Method 3, and the proposed method. The table shows the comparison of three targets: RES curtailment, carbon emission, and operation costs, under four scheduling methods. The proposed strategy performs best in the targets.

MG	Methods	RES Curtailment	Carbon Emission (kg)	Operation Costs (RMB)
MG 1	Method 1	9306	7706	87,188
	Method 2	5733	7299	80,511
	Method 3	6032	7235	72,354
	Proposed method	1638	3291	60,980
MG 2	Method 1	9609	8451	90,123
	Method 2	6249	8058	83,775
	Method 3	6789	7692	78,323
	Proposed method	3343	4321	71,234
MG 3	Method 1	8101	9166	81,354
	Method 2	6432	8849	78,531
	Method 3	7122	7633	77,342
	Proposed method	3760	5323	72,136

4.6. The Analysis of Carbon Trading and Emission

In this section, the carbon emission of different scenarios are analyzed, and the results are shown in Figures 13 and 14. Comparing the two figures, it can be found that the carbon emissions of the three microgrids are significantly lower with the proposed method. This is due to the introduction of the dual-layer energy management strategy, which can effectively reduce carbon emission. It can seen that MG1 has fewer carbon emissions in general. Because the MG1 has the most renewable energy and allocates more free carbon quota. The carbon emission of MG2 and MG3 are somewhat lower in the midday hour compared to other hours. This is because there is more renewable photovoltaic electricity production at midday.

The carbon emissions under different carbon trading prices are given in Figure 15. The change in carbon trading price directly affects the scheduling strategy of interconnected microgrids. The effect of the carbon quota trading price on carbon trading cost is examined.

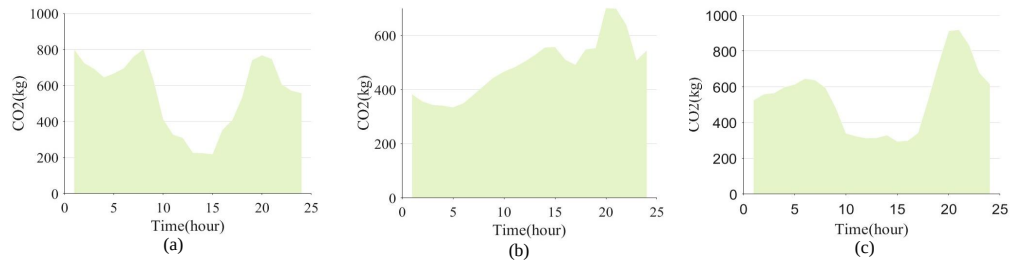

Figure 13. Carbon emission of three microgrids in the interconnected microgrids network without the dual-layer strategy. (**a**) MG1; (**b**) MG2; (**c**) MG3.

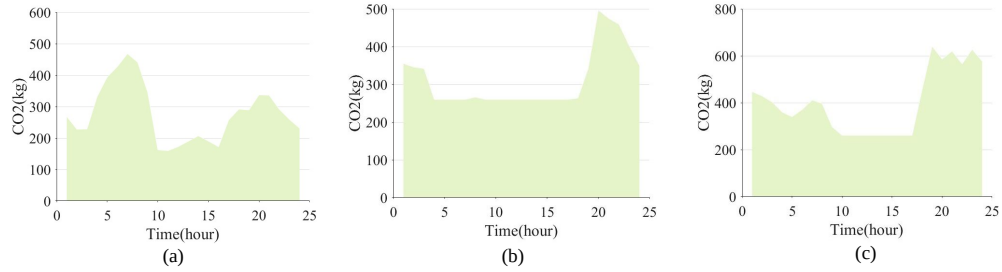

Figure 14. Carbon emission of three microgrids in the interconnected microgrids network with the proposed dual-layer strategy. (**a**) MG1; (**b**) MG2; (**c**) MG3.

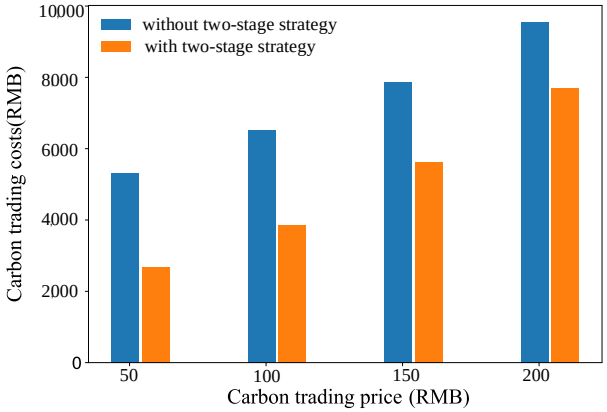

Figure 15. The carbon trading costs under different trading prices with the proposed dual-layer strategy and without the proposed dual-layer strategy.

As the price of carbon quota trading increases, the total cost of carbon trading decreases as the price of carbon trading increases. The reason for this is that the use and coordination of multiple energy sources allow for more flexible scheduling under carbon quota trading. This reduces the need to purchase additional carbon quotas from external carbon markets. Therefore, under carbon quota trading, the dispatching method to reasonably control the carbon emission of microgrids is more beneficial to improve the economy of microgrid operation.

5. Conclusions

This paper presents an integrated energy management strategy for interconnected microgrids, featuring bottom-layer load scheduling and upper-layer energy dispatch with multi-energy sharing and carbon trading. Utilizing an enhanced gray wolf optimization algorithm in the bottom layer for optimal load reallocation and minimizing renewable energy waste, and a distributed alternating direction method of multipliers algorithm in the upper layer for economic and environmental cost minimization, the strategy promotes efficient renewable energy use and low-carbon operations. Simulations validate the benefits of multi-energy sharing and carbon trading, which shows the proposed method's significant performance improvements in microgrid management, with an approximately 41.6% reduction in RES curtailment, about a 41.9% decrease in carbon emissions, and around an 11.3% reduction in operational costs, thus enhancing microgrid economic and environmental advantages.

Future work will be to investigate the impact of dynamic pricing mechanisms on user behavior and grid stability, which have the potential to unlock more responsive and efficient energy consumption patterns. Additionally, ensuring the scalability of our proposed strategy for larger and more complex microgrid networks is a critical factor of future research.

Author Contributions: Conceptualization, J.R. and H.L.; methodology, J.R. and N.T.; software, N.T.; validation, J.R., H.L. and N.T.; formal analysis, J.R. and F.J.; investigation, N.T. and R.Z.; resources, J.R.; data curation, J.R.; writing—original draft preparation, J.R.; writing—review and editing, J.R., N.T. and W.L.; visualization, J.R. and R.Z.; supervision, W.L. and N.T.; project administration, J.R.; funding acquisition, F.J. All authors have read and agreed to the published version of the manuscript.

Funding: This work was funded by the National Science Foundation of China "The Research on Distributed Energy Sharing with Security Guarantee by Cloud Chain Fusion" (Grant No. 62172448).

Data Availability Statement: The raw data supporting the conclusions of this article will be made available by the authors on request.

Conflicts of Interest: The authors declare no conflicts of interest.

Abbreviations

The following abbreviations and nomenclature are used in this manuscript:

RES	Renewable energy source
PV	Photovoltaic
WT	Wind turbine
CHP	Combined heat and power
GB	Gas boiler
ES	Energy storage system
SOC	State-of-charge
CG	Conventional generator
MG	Microgrid
IGWO	Improved gray wolf optimization
ADMM	Alternating direction method of multipliers
Sets	
$\mathcal{N}$	Set of participators
T	Set of time intervals
S	Set of transferable time
Parameters	
$\eta_i^{e,chp}/\eta_i^{h,chp}$	Efficiencies of electricity/heat production for the CHP of microgrid i
$Q_{i,max}^{chp}$	Maximum gas consumption for the CHP
$Q_{i,max}^{gb}$	Maximum gas consumption for the GB
$Q_i^{u,chp}/Q_i^{d,chp}$	Upper/lower bounds of ramp rate limit for the CHP of MG i
$\eta_i^{h,gb}$	Efficiencies of heat production for the GB of MG i
$P_{i,max}^{cg}$	Maximum amounts of electricity of CG of MG i
$P_i^{u,cg}/P_i^{d,cg}$	Upper/lower bounds of ramp rate limit for the CG of MG i
$\eta_i^{es,cp}/\eta_i^{es,d}$	Charging/discharging efficiencies for the storage ES of MG i
$SOC^{es,min}/SOC^{es,max}$	Maximum/minimum SOCs
$\rho_{i,t,s}^{out}/\rho_{i,t,s}^{in}$	Transfers out/in factor
$P_{i-j,t}/H_{i-j,t}$	The electricity/thermal that MG i receives from MG j at time t
Variables	
$W_{i,t}^{o}$	Total carbon quota of MG i
D_{gas}/D_{res}	Carbon quota of gas and res of MG i
$W_{i,t}^{CO_2}$	Carbon emission of MG i
em_i^{gas}/em_i^{oil}	Emission factors of gas and diesel
$P_{i-j,\max}/H_{i-j,\max}$	Maximum electricity/thermal sharing
C_{sys}	Total social operating costs of system
λ_i^{cut}	RES residual price
$Q_{i,t}^{gas}/V_{i,t}^{cg}$	Consumption of gas and diesel of MG
ε	Carbon trading price
$P_{sys,t}^{sur}/P_{sys,t}^{Asur}$	Initial/ actual surplus RES of ith MG
$P_{i,t}^{Oload}$	Initial electric load of MG i
$C_{sys,t}^{\text{res}}$	The surplus RES costs of system

$P_{i,t}^{Aload}$	Actual electric load of MG i
$P_{i,t}^{cutRES}$	RES power cut of MG i at time step t
λ_{oil}	Diesel fuel prices
$C_{i,t}^{cutRES}$	RES cut costs
$C_{sys,t}^{\text{dissatisfaction}}$	User dissatisfaction of system
a	IGWO nonlinear convergence factor
Cauchy()	Cauchy function
$C_{BottomLayer}$	Optimization cost of the bottom layer
$P_{i,t}^{chp}$	Electricity production for CHP
$H_{i,t}^{chp}$	Heat production for the CHP
$Q_{i,t}^{GB}$	Gas consumption for GB
$P_{i,t}^{pv}$	PV power of ith MG at time t
$P_{i,t}^{wt}$	WT power of ith MG at time t
$Q_{i,t}^{chp}$	Gas consumption for CHP
$P_{i,t}^{cg}$	Electricity production for CG
$P_{i,t}^{es,ch}$	Charging rates for ES
$P_{i,t}^{es,dch}$	Discharging rates for ES
$P_{i,t,s}^{sche,out}$ / $P_{i,t,s}^{sche,in}$	Electrical power transferred out/in

References

1. Li, G. Revolutionizing energy management: A two-step optimal day-ahead scheduling approach for advanced distribution systems with enhanced transactional efficiency. *Comput. Electr. Eng.* **2024**, *117*, 109291. [CrossRef]
2. Jirdehi, M.A.; Tabar, V.S.; Zadeh, S.G.; Tohidi, S. Different aspects of microgrid management: A comprehensive review. *J. Energy Storage* **2020**, *30*, 101457. [CrossRef]
3. Li, Z.; Xu, Y. Optimal coordinated energy dispatch of a multi-energy microgrid in grid-connected and islanded modes. *Appl. Energy* **2018**, *210*, 974–986. [CrossRef]
4. A comprehensive review of energy management and planning of islanded microgrids: Part 1—Optimization formulations. *CSEE J. Power Energy Syst.* **2019**, *6*, 329–343. [CrossRef]
5. Yoldaş, Y.; Önen, A.; Muyeen, S.; Vasilakos, A.V.; Alan, I. Enhancing smart grid with microgrids: Challenges and opportunities. *Renew. Sustain. Energy Rev.* **2017**, *72*, 205–214. [CrossRef]
6. Rezaei, N.; Pezhmani, Y. Optimal islanding operation of hydrogen integrated multi-microgrids considering uncertainty and unexpected outages. *J. Energy Storage* **2022**, *49*, 104142. [CrossRef]
7. Elsheakh, Y.; Zou, S.; Ma, Z.; Zhang, B. Decentralised gradient projection method for economic dispatch problem with valve point effect. *IET Gener. Transm. Distrib.* **2018**, *12*, 3844–3851. [CrossRef]
8. Ma, Y.; Xu, W.; Yang, H.; Zhang, D. Two-stage stochastic robust optimization model of microgrid day-ahead dispatching considering controllable air conditioning load. *Int. J. Electr. Power Energy Syst.* **2022**, *141*, 108174. [CrossRef]
9. Wang, T.; Wang, J.; Zhao, Y.; Shu, J.G.; Chen, J. Multi-objective residential load dispatch based on comprehensive demand response potential and multi-dimensional user comfort. *Electr. Power Syst. Res.* **2023**, *220*, 109331. [CrossRef]
10. Mota, B.; Faria, P.; Vale, Z.A. Residential load shifting in demand response events for bill reduction using a genetic algorithm. *Energy* **2022**, *260*, 124978. [CrossRef]
11. Wang, C.; Ge, P.; Sun, L.; Wang, F. Research on user-side flexible load scheduling method based on greedy algorithm. *Energy Rep.* **2022**, *8*, 192–201. [CrossRef]
12. Chen, Z.; Chen, Y.; He, R.; Liu, J.; Gao, M.; Zhang, L. Multi-objective residential load scheduling approach for demand response in smart grid. *Sustain. Cities Soc.* **2021**, *76*, 103530. [CrossRef]
13. Pradhan, M.; Roy, P.K.; Pal, T. Grey wolf optimization applied to economic load dispatch problems. *Int. J. Electr. Power Energy Syst.* **2016**, *83*, 325–334. [CrossRef]
14. Mirjalili, S.; Mirjalili, S.M.; Lewis, A. Grey Wolf Optimizer. *Adv. Eng. Softw.* **2014**, *69*, 46–61. [CrossRef]
15. Deng, H.; Wang, J.; Shao, Y.; Zhou, Y.; Cao, Y.; Zhang, X.; Li, W. Optimization of configurations and scheduling of shared hybrid electric hydrogen energy storages supporting to multi-microgrid system. *J. Energy Storage* **2023**, *74*, 109420. [CrossRef]
16. Gao, H.; Hu, M.; He, S.; Liu, J. Green electricity trading driven low-carbon sharing for interconnected microgrids. *J. Clean. Prod.* **2023**, *414*, 137618. [CrossRef]
17. Wang, H.; Huang, J. Incentivizing Energy Trading for Interconnected Microgrids. *IEEE Trans. Smart Grid* **2016**, *9*, 2647–2657. [CrossRef]
18. Jithendranath, J.; Das, D. Stochastic planning of islanded microgrids with uncertain multi-energy demands and renewable generations. *IET Renew. Power Gener.* **2021**, *14*, 4179–4192. [CrossRef]

19. Zia, M.F.; Elbouchikhi, E.; Benbouzid, M. Microgrids energy management systems: A critical review on methods, solutions, and prospects. *Appl. Energy* **2018**, *222*, 1033–1055. [CrossRef]
20. Li, Q.; Gao, D.W.; Zhang, H.; Wu, Z.; Wang, F. Consensus-Based Distributed Economic Dispatch Control Method in Power Systems. *IEEE Trans. Smart Grid* **2019**, *10*, 941–954. [CrossRef]
21. Qiu, H.; You, F. Decentralized-distributed robust electric power scheduling for multi-microgrid systems. *Appl. Energy* **2020**, *269*, 115146. [CrossRef]
22. Mohamed, M.A.; Jin, T.; Su, W. Multi-agent energy management of smart islands using primal-dual method of multipliers. *Energy* **2020**, *208*, 118306. [CrossRef]
23. Peng, Q.; Low, S.H. Distributed Optimal Power Flow Algorithm for Radial Networks, I: Balanced Single Phase Case. *IEEE Trans. Smart Grid* **2018**, *9*, 111–121. [CrossRef]
24. Fang, X.; Hodge, B.M.S.; Jiang, H.; Zhang, Y.Y. Decentralized wind uncertainty management: Alternating direction method of multipliers based distributionally-robust chance constrained optimal power flow. *Appl. Energy* **2019**, *239*, 938–947. [CrossRef]
25. Xiang, Y.; Cai, H.; Gu, C.; Shen, X. Cost-benefit analysis of integrated energy system planning considering demand response. *Energy* **2020**, *192*, 116632. [CrossRef]
26. Korkas, C.D.; Baldi, S.; Michailidis, I.T.; Kosmatopoulos, E.B. Occupancy-based demand response and thermal comfort optimization in microgrids with renewable energy sources and energy storage. *Appl. Energy* **2016**, *163*, 93–104. [CrossRef]
27. Bıyık, E.; Kahraman, A. A predictive control strategy for optimal management of peak load, thermal comfort, energy storage and renewables in multi-zone buildings. *J. Build. Eng.* **2019**, *25*, 100826. [CrossRef]
28. Wamalwa, F.; Ishimwe, A. Optimal energy management in a grid-tied solar PV-battery microgrid for a public building under demand response. *Energy Rep.* **2024**, *12*, 3718–3731. [CrossRef]
29. Setlhaolo, D.; Xia, X. Combined residential demand side management strategies with coordination and economic analysis. *Int. J. Electr. Power Energy Syst.* **2016**, *79*, 150–160. [CrossRef]
30. Lin, C.C.; Deng, D.J.; Kuo, C.C.; Liang, Y.L. Optimal Charging Control of Energy Storage and Electric Vehicle of an Individual in the Internet of Energy With Energy Trading. *IEEE Trans. Ind. Inform.* **2018**, *14*, 2570–2578. [CrossRef]
31. Wang, K.; Liang, Y.; Jia, R.; Wu, X.; Wang, X.; Dang, P. Two-stage stochastic optimal scheduling for multi-microgrid networks with natural gas blending with hydrogen and low carbon incentive under uncertain envinronments. *J. Energy Storage* **2023**, *72*, 108319. [CrossRef]
32. Yang, K.; Li, C.; Jing, X.; Zhu, Z.; Wang, Y.; Ma, H.; Zhang, Y. Energy dispatch optimization of islanded multi-microgrids based on symbiotic organisms search and improved multi-agent consensus algorithm. *Energy* **2022**, *239*, 122105. [CrossRef]
33. Saremi, S.; Mirjalili, S.Z.; Mirjalili, S.M. Evolutionary population dynamics and grey wolf optimizer. *Neural Comput. Appl.* **2015**, *26*, 1257–1263. [CrossRef]
34. Faris, H.; Aljarah, I.; Al-Betar, M.A.; Mirjalili, S. Grey wolf optimizer: A review of recent variants and applications. *Neural Comput. Appl.* **2018**, *30*, 413–435. [CrossRef]
35. Kohli, M.; Arora, S. Chaotic grey wolf optimization algorithm for constrained optimization problems. *J. Comput. Des. Eng.* **2018**, *5*, 458–472. [CrossRef]
36. Nahiduzzaman, M. *Expert Systems with Applications*; Elsevier: Amsterdam, The Netherlands, 2022.
37. Li, B.; Wang, H.; Wang, X.; Negnevitsky, M.; Li, C. Tri-stage optimal scheduling for an islanded microgrid based on a quantum adaptive sparrow search algorithm. *Energy Convers. Manag.* **2022**, *261*, 115639. [CrossRef]
38. Wilson, E.J.; Parker, A.; Fontanini, A. *Evaluacion del Potencial Solar Fotovoltaico en Brownfields y Embalses de Puerto Rico: Analisis y Modelaje*; Technical Report; National Renewable Energy Lab. (NREL): Golden, CO, USA, 2024.
39. Wilson, E.J.; Parker, A. *Wind Turbine Design Guideline DG03: Yaw and Pitch Bearings*; Technical Report; National Renewable Energy Lab. (NREL): Golden, CO, USA, 2024.
40. Wilson, E.J.; Parker, A.; Fontanini, A.; Present, E.; Reyna, J.L.; Adhikari, R.; Bianchi, C.; CaraDonna, C.; Dahlhausen, M.; Kim, J.; et al. *End-Use Load Profiles for the US Building Stock: Methodology and Results of Model Calibration, Validation, and Uncertainty Quantification*; Technical Report; National Renewable Energy Lab. (NREL): Golden, CO, USA, 2022.
41. Zheng, J.; Du, J.; Wang, B.; Klemeš, J.J.; Liao, Q.; Liang, Y. A hybrid framework for forecasting power generation of multiple renewable energy sources. *Renew. Sustain. Energy Rev.* **2023**, *172*, 113046. [CrossRef]
42. Qiu, D.; Dong, Z.; Zhang, X.; Wang, Y.; Strbac, G. Safe reinforcement learning for real-time automatic control in a smart energy-hub. *Appl. Energy* **2022**, *309*, 118403. [CrossRef]
43. Qiu, D.; Xue, J.; Zhang, T.; Wang, J.; Sun, M. Federated reinforcement learning for smart building joint peer-to-peer energy and carbon allowance trading. *Appl. Energy* **2023**, *333*, 120526. [CrossRef]
44. Choi, Y.C. Dispatching rule-based scheduling algorithms in a single machine with sequence-dependent setup times and energy requirements. *Procedia CIRP* **2016**, *41*, 135–140. [CrossRef]